

# Metal(II) Formates (M = Fe, Co, Ni, and Cu) Stabilized by Tetramethylethylenediamine (tmeda): Convenient Molecular Precursors for the Synthesis of Supported Nanoparticles

## Journal Article

### Author(s):

Margossian, Tigran; [Larmier, Kim](#) ; Allouche, Florian; [Chan, Ka Wing](#) ; [Copéret, Christophe](#) 

### Publication date:

2019-04

### Permanent link:

<https://doi.org/10.3929/ethz-b-000340406>

### Rights / license:

[In Copyright - Non-Commercial Use Permitted](#)

### Originally published in:

Helvetica Chimica Acta 102(4), <https://doi.org/10.1002/hlca.201800227>

# Metal(II) formates (M = Fe, Co, Ni and Cu) stabilized by tetramethylethylenediamine (tmeda): Convenient Molecular Precursors for the Synthesis of Supported Nanoparticles

Tigran Margossian<sup>a</sup>, Kim Larmier<sup>a</sup>, Florian Allouche<sup>a</sup>, Ka Wing Chan<sup>a</sup>, Christophe Copéret<sup>\*a</sup>

<sup>a</sup> Department of Chemistry and Applied Biosciences, Vladimir Prelog Web. 1-5 ETH Zurich, CH-8093 Zurich, Switzerland

$\gamma$ -Alumina supported 3d transition-metal nanoparticles are commonly used catalysts for several industrial reactions such as Fischer-Tropsch, reforming, methanation and hydrogenation reactions. However, the activity of such catalyst is often limited by the low metal dispersion and a high content of irreducible metal, inherent to the conventional preparation methods in aqueous phase. In this context, we have recently shown that  $[\{\text{Ni}(\mu^2\text{-OCHO})(\text{OCHO})(\text{tmeda})\}_2(\mu^2\text{-OH}_2)]$  (tmeda = tetramethylethylenediamine) is a suitable molecular precursor for the formation of 1-2 nm large nanoparticles onto alumina. Here, we explore the synthesis of the corresponding Fe, Co and Cu molecular precursors, namely  $[\{\text{Fe}(\mu^2\text{-OCHO})(\text{OCHO})(\text{tmeda})\}_4]$ ,  $[\{\text{Co}(\mu^2\text{-OCHO})(\text{OCHO})(\text{tmeda})\}_2(\mu^2\text{-OH}_2)]$ ,  $[\text{Cu}(\kappa^2\text{-OCHO})_2(\text{tmeda})]$ , which are, like the Ni precursor, soluble in a range of solvents, rendering them convenient metal precursors for the preparation of supported metallic nanoparticles on  $\gamma$ -alumina. Using a specific adsorption of the molecular precursor on  $\gamma$ -alumina in a suitable organic solvent, treatment under  $\text{H}_2$  provides small and narrowly distributed Fe ( $2.5 \pm 0.9$  nm), Co ( $3.0 \pm 1.2$  nm), Ni ( $1.7 \pm 0.5$  nm) and Cu ( $2.1 \pm 1.5$  nm) nanoparticles. XAS shows that the proportion of  $\text{MAl}_2\text{O}_4$  (M = Co, Ni, Cu) is small, thus illustrating the advantage of using these tailor-made molecular precursors.

**Keywords:** Metal formate, tetramethylethylenediamine•Specific adsorption•Metal(0) nanoparticles

## Introduction

Metal supported nanoparticles are the most common heterogeneous catalyst used in industry.<sup>[1-3]</sup> They are used in a broad range of applications, such as methane conversion processes,<sup>[4-9]</sup> biomass transformation<sup>[10, 11]</sup> or fine chemical synthesis.<sup>[12, 13]</sup> Numerous parameters influence the performances of these catalysts, such as the type of support,<sup>[14, 15]</sup> the metal nanoparticles size,<sup>[16, 17]</sup> and their interaction with the support.<sup>[18-21]</sup> Decreasing the size of those supported nanoparticles allows the enhancement of catalyst performances.<sup>[7, 16, 18, 22-24]</sup> While small particles and good dispersion can be obtained on various supports, a significant fraction of metal can be lost through its incorporation into the support through the formation of hardly reducible metal-aluminum mixed oxides in the case of alumina.<sup>[25-27]</sup> The reduction of such metal incorporated into the support during the impregnation phase requires the use of high temperature treatment under reductive atmosphere, leading typically to severe sintering of the particles, with nanoparticle size possibly exceeding 10 nm for Cu, Ni and Co, up to 80 nm for Fe.<sup>[28-33]</sup> Several approaches have been undertaken to avoid these problems, for instance, by modifying conventional preparation methods by either complexing the initial molecular precursor with a chelating ligand<sup>[34-38]</sup> or by adding precious metal to the material.<sup>[17, 39, 40]</sup> This allows for a drop of the reduction temperature and hence the decrease of particle size. We have recently introduced a Ni formate –  $[\{\text{Ni}(\mu^2\text{-OCHO})(\text{OCHO})(\text{tmeda})\}_2(\mu^2\text{-OH}_2)]$  (**[Ni]**) (tmeda = tetramethylethylenediamine) – as a convenient molecular precursor for the synthesis of 1-2 nm Ni(0) on a broad range of supports via a specific adsorption method in organic solvent followed by a reduction step under H<sub>2</sub>.<sup>[7, 18]</sup> We reasoned that it would be valuable to broaden this approach to other 3d transition metals, namely Fe, Co and Cu, because of their relatively low cost and use in numerous applications.<sup>[41-45]</sup> Here, we describe the synthesis of metal formate  $[\{\text{Fe}(\mu^2\text{-OCHO})(\text{OCHO})(\text{tmeda})\}_4]$  (**[Fe]**),  $[\{\text{Co}(\mu^2\text{-OCHO})(\text{OCHO})(\text{tmeda})\}_2(\mu^2\text{-OH}_2)]$  (**[Co]**),  $[\text{Cu}(\kappa^2\text{-OCHO})_2(\text{tmeda})]$  (**[Cu]**) as precursors for the synthesis of the supported nanoparticles, here using alumina as a prototypical support, commonly used in industry<sup>[46-48]</sup> that typically suffers from incorporation of the metal ions into its structure, hence the need of high temperature of reduction to generate metal nanoparticles.

## Results and Discussion

Fe(II), Co(II) and Cu(II) formate compounds – **[Fe]**, **[Co]**, **[Cu]** – were prepared from readily available metal precursors via the same strategy as previously reported for **[Ni]** using tmeda<sup>[71]</sup> ( as a stabilizing ligand (Scheme 1). The yields are 34 % and 75 %, for ([{Co( $\mu^2$ -OCHO)(OCHO)(tmeda)}<sub>2</sub>( $\mu^2$ -OH<sub>2</sub>)] **[Co]** and [Cu( $\kappa^2$ -OCHO)<sub>2</sub>(tmeda)] **[Cu]**, respectively, while **[Fe]**, a sensitive compound prepared under inert conditions, is obtained in 33 % yield. All syntheses can be carried out on a multi-gram scale to give pure crystalline complex soluble in a range of solvent from water to toluene (Table S1). While they all display similar structural features, in particular a +2 oxidation state and the presence of octahedral metal sites, they differ by their nuclearity: mono and tetra-nuclear for **[Cu]** and **[Fe]** vs. dinuclear for **[Co]** as found for the previously reported **[Ni]** complexes. The tmeda ligand is connected in the same  $\eta^2$  mode for the four different structures. The M<sub>1</sub>-N<sub>1</sub>(or M<sub>1</sub>-N<sub>2</sub>) bond distances decrease from 2.295(2) Å for **[Fe]** to 2.192(2) Å for **[Co]**, 2.168(2) Å for **[Ni]** and 2.028(2) Å for **[Cu]** following the decrease size in metal ionic radius for the Fe<sup>2+</sup>, Co<sup>2+</sup> and Ni<sup>2+</sup> (Table 1).<sup>[49]</sup> The N<sub>1</sub>-M<sub>1</sub>-N<sub>2</sub> angle also increases from 80.04(8) deg to 87.13(8) deg on going from **[Fe]** to **[Cu]**. Overall, their solid-state structure follows the size of the metal: with Fe<sup>2+</sup>, the larger cation of the series, the compound adopts a tetrameric structure (Figure 1a), while the structures are dimeric or monomeric with smaller M<sup>2+</sup> ions (M = Co, Ni and Cu) sa shown in Figure 1b-d.

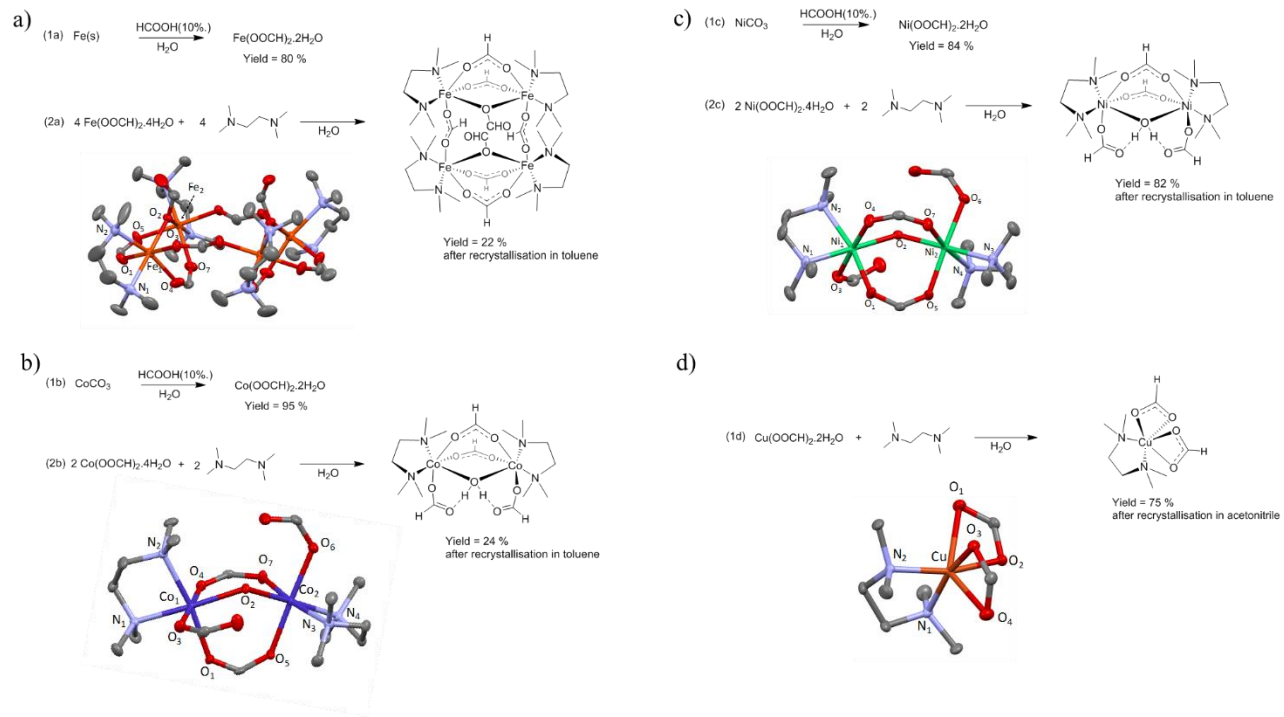


**Figure 1.** Crystal structure and synthesis path of complex a)[Fe], b)[Co], c)[Ni], d)[Cu]. Thermal ellipsoids were set at 50% probability level and except for  $\mu\text{-H}_2\text{O}$  for complex [Co] and [Ni], hydrogen atoms and the co-crystallized water molecule are omitted for clarity.<sup>[50]</sup>

**Table 1.** Summary of the Bond Distances and Angles from X-ray Crystallography of the different complexes.

	[Fe]	[Co]	[Ni]	[Cu]
Distances				
M2+radius <sup>[51]</sup>	0.92 <sup>a</sup>	0.89 <sup>a</sup>	0.83	0.87
M1-O1	2.095(2)	2.075(2)	2.049(2)	2.499(2)
M1-O2	2.171(1)	2.150(1)	2.099(1)	1.992(1)
M1-N1	2.295(2)	2.192(2)	2.168(2)	2.028(2)
M1-N2	2.275(2)	2.207(2)	2.148(2)	2.028(2)

<sup>a</sup> a: High spin ionic radius, evidenced by UV-VIS for [Co] (Figure 3).

Specific adsorption of the different precursors onto dehydroxilated  $\gamma$ -alumina was conducted with an equimolar quantity of precursor with respect to surface –OH (except for [Fe]), using toluene for [Co] and [Ni] vs. acetonitrile for [Fe] and [Cu] in order to take into account their specific solubility (Table S1). After washing the excess of complex and drying, the metal loading of the different specifically adsorbed precursors was measured by elemental analysis. The metal loading of Fe/Al<sub>2</sub>O<sub>3</sub> is 0.82 wt% for a measured surface area of alumina of 32 m<sup>2</sup>.g<sup>-1</sup>, corresponding to 2.9 metal.nm<sup>-2</sup> for Fe/Al<sub>2</sub>O<sub>3</sub>. As shown on Figure 2, the metal loading decreases for the other metals with 2.4 metal.nm<sup>-2</sup> for Co/Al<sub>2</sub>O<sub>3</sub>, 1.8 metal.nm<sup>-2</sup> for Ni/Al<sub>2</sub>O<sub>3</sub> and 1 metal.nm<sup>-2</sup> for Cu/Al<sub>2</sub>O<sub>3</sub>. Noteworthy the precursor loading expressed in number of precursor per nm<sup>2</sup> is similar for all system, close to unity with 0.7 [Fe].nm<sup>-2</sup>, 1.2 [Co].nm<sup>-2</sup>, 0.9 [Ni].nm<sup>-2</sup> and 1.0 [Cu].nm<sup>-2</sup>, in line with approximately 2 OH.nm<sup>-2</sup> per precursor (Figure 2, red columns).<sup>[52]</sup>

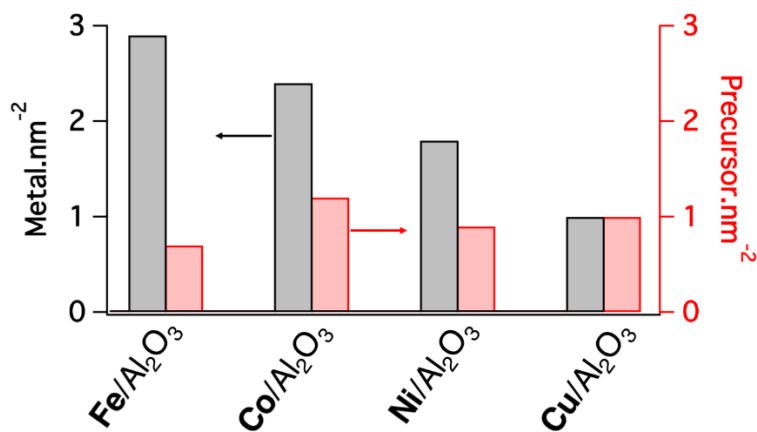


**Figure 2.** Metal uptake (right column, black) onto Al<sub>2</sub>O<sub>3-500</sub> and precursor uptake (left column, red) onto Al<sub>2</sub>O<sub>3-500</sub>, which corresponds to the metal loading divided by the number of metal atoms per molecular complex.

The structure of the different adsorbed species onto  $\gamma$ -alumina was thus investigated by a combination of spectroscopies (IR, UV-Vis, XAS). The IR spectra of the different specifically adsorbed complexes onto Al<sub>2</sub>O<sub>3-500</sub> recorded under argon are shown in Figure S3. We observe that the specific adsorption of the different precursors induces a shift of the Al-OH bands to lower wavenumbers and to the appearance of Csp<sup>2</sup>-H, Csp<sup>3</sup>-H and C-O bands associated with the formate and tmeda ligands, with bands at 2980 cm<sup>-1</sup>, 2849 cm<sup>-1</sup>, 2731 cm<sup>-1</sup>, 1610 cm<sup>-1</sup> and 1470 cm<sup>-1</sup>. According to X-ray absorption spectroscopy (XAS), the edge energy decreases from 7120.0 eV for [Fe] to 7112.0 eV for Fe/Al<sub>2</sub>O<sub>3</sub> (measured from the first inflection point of the spectra), which indicates reduction of Fe centers. However, obtaining information on the coordination environment was not possible due to poor data quality of the extended X-ray absorption fine structure (EXAFS). Linear combination fitting of the Fe/Al<sub>2</sub>O<sub>3</sub> XANES spectra shows 45 % of [Fe] (Fe<sup>2+</sup>), 34 % of Fe<sub>2</sub>O<sub>3</sub> (Fe<sup>3+</sup>) and 21 % of Fe foil (Fe<sup>0</sup>, Figure S4). This complex mixture of Fe species lead us to hypothesize that [Fe] partially disproportionate to iron (0) metal and iron oxide (III) upon contact onto the alumina surface according to an equation of the type:  $3 \text{Fe}^{2+} \rightarrow \text{Fe}^0 + 2 \text{Fe}^{3+}$ .

The adsorption of **[Co]** onto alumina surface was studied with a similar approach. UV-Vis spectrum of **[Co]**-complex shows a unique band at 510 nm that can be assigned to the d-d transition of an octahedral  $\text{Co}^{2+}(\text{d}^7)$ .<sup>[37]</sup> However, **Co/Al<sub>2</sub>O<sub>3</sub>** shows one red-shifted bands at 558 (Figure 3a) by comparison to what is observed for **[Co]**. This is consistent with the coordination of **[Co]** onto the surface hydroxyl groups of alumina as previously observed for Ni.<sup>[7, 25, 36]</sup> While a change of oxidation state and/or of the geometry could also explain this observation,<sup>[37, 53]</sup> the XANES spectra of **[Co]** and **Co/Al<sub>2</sub>O<sub>3</sub>** (Figure S5) show similar edge energies (7719.8 eV and 7720.3 eV, respectively), consistent with the conservation of the Co(II) oxidation state upon dispersion in this case. Furthermore, the absence of a pre-edge features in both spectra indicates that Co remains octahedral upon adsorption. EXAFS spectra and fits for **[Co]** and **Co/Al<sub>2</sub>O<sub>3</sub>** are shown in Figure S6. In the case of the molecular precursor, the fit includes scattering paths of four closest oxygen atoms, two nitrogen atoms, nine carbon atoms from the second sphere, and the other cobalt center. The bond distances obtained from the fit of **[Co]** are consistent with its X-ray structure (Table S2 and Table 1). The best fit of **Co/Al<sub>2</sub>O<sub>3</sub>** is obtained by keeping the octahedral geometry of the initial precursor and by adding one Co-Al scattering path with 2 aluminum neighbors accounts for two features at 2.86 Å, consistent with a surface coordination complex. A cobalt-cobalt path allows to fit the feature centered at 3.61 Å (Figure S6-S8). This suggests that **[Co]** retains its dimeric structure at the surface of alumina (Figure 4).

The UV-vis spectrum of (**Cu/Al<sub>2</sub>O<sub>3</sub>**) shares similarities with that of **[Cu]** (Figure 3c), showing bands at 270 nm and 650 nm that can be assigned to charge transfer and d-d of a distorted octahedral  $\text{Cu}^{2+}(\text{d}^9)$ .<sup>[54]</sup> The d-d band of **Cu/Al<sub>2</sub>O<sub>3</sub>** is red-shifted in comparison to the **[Cu]**-complex, which is ascribed to a weaker field ligand environment at the metal such as  $\text{Al}_2\text{O}_3$ .<sup>[7, 55]</sup> Despite the **[Cu]**-complex and **Cu/Al<sub>2</sub>O<sub>3</sub>** can not be studied by XAS due to the reduction of Cu centers under the X-Ray beam, **[Cu]** likely retains its octahedral structure after adsorption on alumina surface, based on the UV-visible analysis.



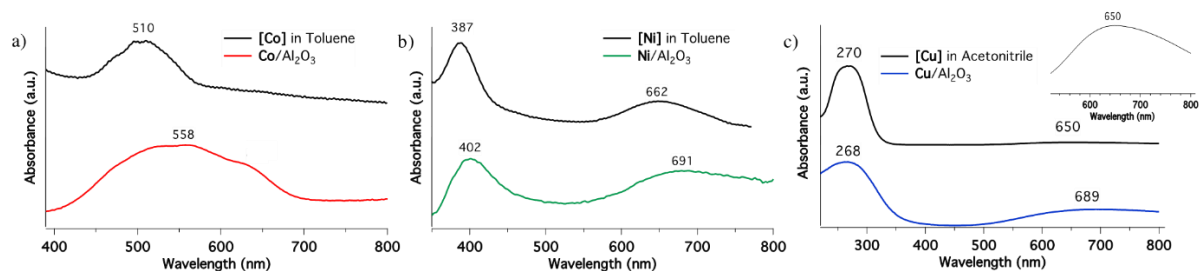


**Figure 3.** Background subtracted UV-Vis spectra of materials (a) Co/Al<sub>2</sub>O<sub>3</sub> and [Co] in toluene solution, (b) Ni/Al<sub>2</sub>O<sub>3</sub> and [Ni] in toluene solution, (c) Cu/Al<sub>2</sub>O<sub>3</sub> and [Cu] in acetonitrile solution

When the different metal formate complexes are specifically adsorbed onto  $\gamma$ -alumina surface, they retain their octahedral conformation for [Co] and [Cu] as previously observed<sup>[7]</sup> and re-confirmed for [Ni] by UV-VIS spectroscopy (Figure 3). In addition, like for Ni, the Co complex retains its dimeric structure upon chemisorption onto  $\gamma$ -alumina surface (Figure 4a and 4b).

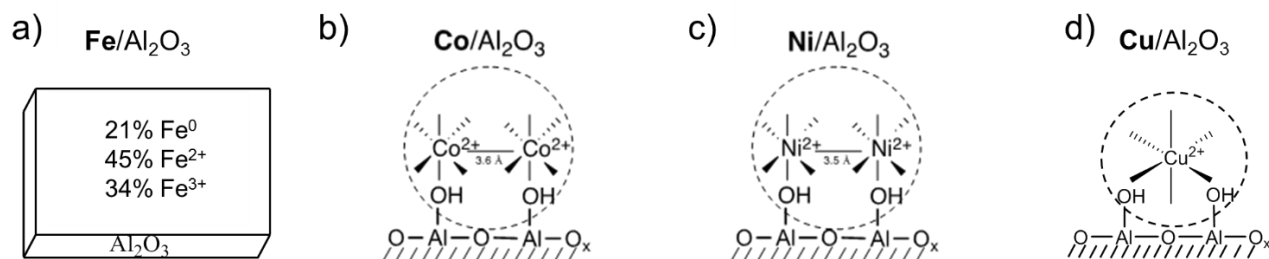


**Figure 4.** Surface coordination complex for (a) Fe/Al<sub>2</sub>O<sub>3</sub>, (b) Co/Al<sub>2</sub>O<sub>3</sub>, (c) Ni/Al<sub>2</sub>O<sub>3</sub> (d) Cu/Al<sub>2</sub>O<sub>3</sub>

Following the specific adsorption of the different metal precursor onto the alumina surface, reduction at 700 °C in hydrogen flow yields nanoparticles with particle size distribution of  $2.5 \pm 0.8$  nm for Fe<sub>700</sub> (Figure 5a),  $3.0 \pm 1.2$  nm for Co<sub>700</sub> (Figure 5b), of  $1.7 \pm 0.5$  nm for Ni<sub>700</sub> (Figure 5c) and of  $4.5 \pm 2.2$  nm for Cu<sub>700</sub> (Figure 5d). Smaller and narrower particle size distribution can also be achieved in the case of

copper when decreasing the reduction temperature down to 500 °C with an average size of  $2.1 \pm 1.5$  nm (**Cu<sub>500</sub>**, Figure S14).

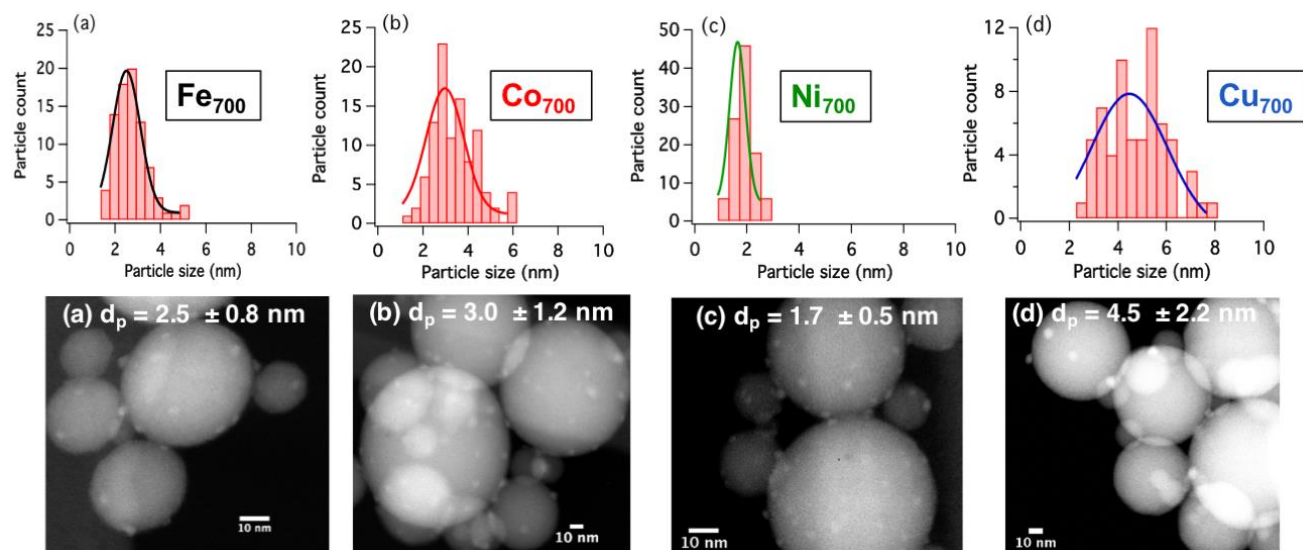


**Figure 5.** Particle distribution function of the particle size associated to the TEM pictures for the alumina-based catalyst

**Table 2.** Characterization of the as prepared supported nanoparticle catalysts. The alumina supports were dehydroxylated at 500 °C

Precursor	Solvent	Impregnate material	Reduced material <sup>a</sup>	Metal <sup>b</sup> (% wt)	Metal density	Particle size <sup>c</sup> (nm)	XANES analysis <sup>d</sup> (%)	LCF
-----------	---------	---------------------	-------------------------------	------------------------------	---------------	------------------------------------	------------------------------------	-----

					(Metal.nm <sup>-2</sup> )		M(0)	MAI <sub>2</sub> O <sub>4</sub>
[Fe]	CH <sub>3</sub> CN	<b>Fe</b> /Al <sub>2</sub> O <sub>3</sub>	Fe <sub>700</sub>	0.82	2.9	2.5 ± 0.9	40	20(40) <sup>e</sup>
[Fe]	CH <sub>3</sub> CN	<b>Fe</b> /Al <sub>2</sub> O <sub>3</sub>	Fe <sub>900</sub>	0.82	2.9	7.8 ± 3.0	n.d.	n.d.
[Co]	Toluen e	<b>Co</b> /Al <sub>2</sub> O <sub>3</sub>	Co <sub>700</sub>	0.80	2.4	3.0 ± 1.2	80	20
[Ni]	Toluen e	<b>Ni</b> /Al <sub>2</sub> O <sub>3</sub>	Ni <sub>700</sub>	0.58	1.8	1.7 ± 0.5	92	8
[Cu]	CH <sub>3</sub> CN	<b>Cu</b> /Al <sub>2</sub> O <sub>3</sub>	Cu <sub>500</sub>	0.34	1	2.1 ± 1.5	n.d.	n.d.
[Cu]	CH <sub>3</sub> CN	<b>Cu</b> /Al <sub>2</sub> O <sub>3</sub>	Cu <sub>700</sub>	0.34	1	4.5 ± 2.2	98	2

a: Fe<sub>700</sub> correspond to Fe/Al<sub>2</sub>O<sub>3</sub> reduced at 700 °C b: Metal loading determined by elemental analysis; c: measured by HAADF/STEM d: Determined by Linear Combination Fitting of the XANES spectrum using the corresponding spinel (MAI<sub>2</sub>O<sub>4</sub>) and foil references; e: for Fe<sub>700</sub> LCF an additional Fe<sub>2</sub>O<sub>3</sub> reference was used with (value).

Depending on the metal precursor specifically adsorbed on the surface, formation and size of the particles are influenced by the reduction temperature and hence, the reducibility of the different systems was estimated by XANES analysis at the respective metal edge after reduction of the samples at 700 °C (Figure 6). The XANES spectra of **Co**<sub>700</sub>, **Ni**<sub>700</sub> and **Cu**<sub>700</sub> (Figure 6 a, b, c) are very similar to that of their respective metal foil reference, displaying similar pre-edge and edge positions. In contrast, the XANES

spectrum of  $\text{Fe}_{700}$  contains a white line with a normalized adsorption value that is 50 % higher than that of the Fe foil reference, indicative of the presence of oxidized iron species. Linear combination fitting of the XANES data for  $\text{Fe}_{700}$  using the Fe foil,  $\text{FeAl}_2\text{O}_4$  and  $\text{Fe}_2\text{O}_3$  references (Figure 6a) showing that only 40 % of total iron was reduced at 700 °C under an  $\text{H}_2$  flow. While reducing at 900 °C would likely help to fully reduce the oxidized iron, it has a detrimental effect on particle size, which increases from 2.5 to 7.8 nm. LCF analysis of the XANES data for the three other systems reduced at 700 °C shows that the metal(0) content increases, while moving from left to right in the periodic table with 80 % for  $\text{Co}_{700}$ , 92 % for  $\text{Ni}_{700}$  and 98 % for  $\text{Cu}_{700}$ . This is directly in line with the Temperature Programmed Reduction study (Figure S17). After reduction at 700 °C, the proportion of fully reduced metal increases from iron to copper (Figure 7 and Table 2).

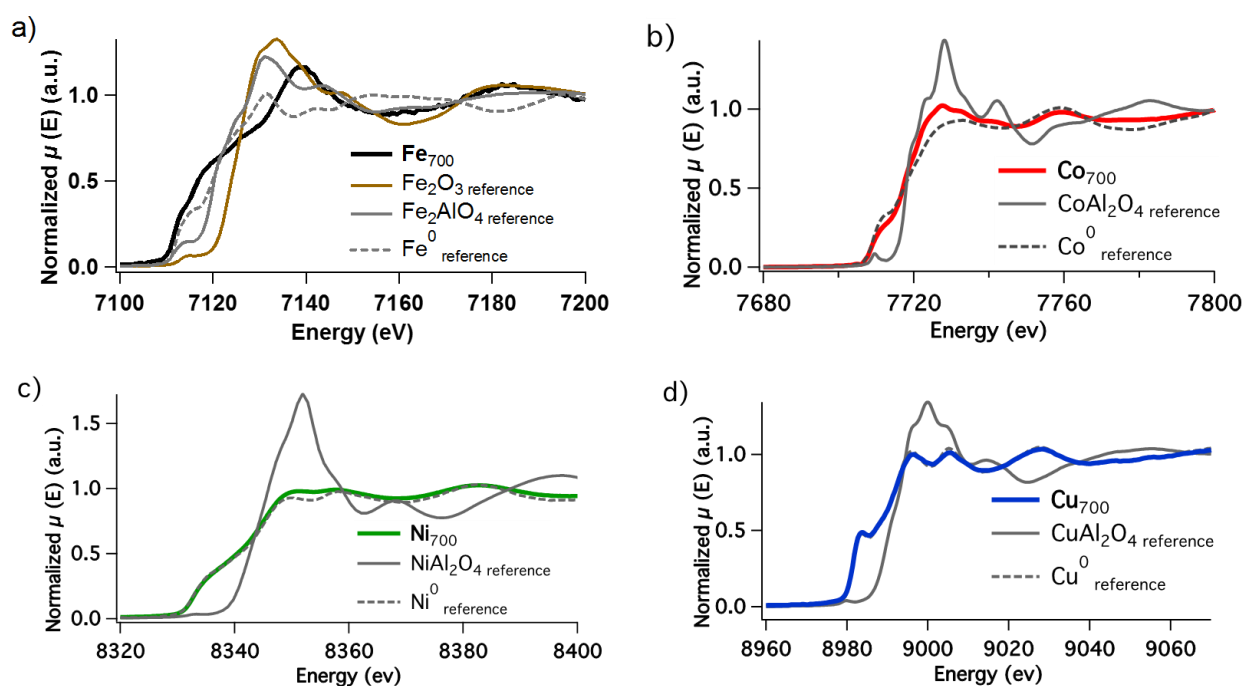


**Figure 6.** XANES spectrum for the different reduced samples; (a) Fe K-edge:  $\text{Fe}_{700}$ ,  $\text{FeAl}_2\text{O}_4$ ,  $\text{Fe}_2\text{O}_3$  and  $\text{Fe}^0$  reference, (b) Co K-edge:  $\text{Co}_{700}$ ,  $\text{CoAl}_2\text{O}_4$  and  $\text{Co}^0$  reference, (c) Ni K-edge:  $\text{Ni}_{700}$ ,  $\text{NiAl}_2\text{O}_4$  and  $\text{Ni}^0$  reference, (d) Cu K-edge:  $\text{Cu}_{700}$ ,  $\text{CuAl}_2\text{O}_4$  and  $\text{Cu}^0$  reference.

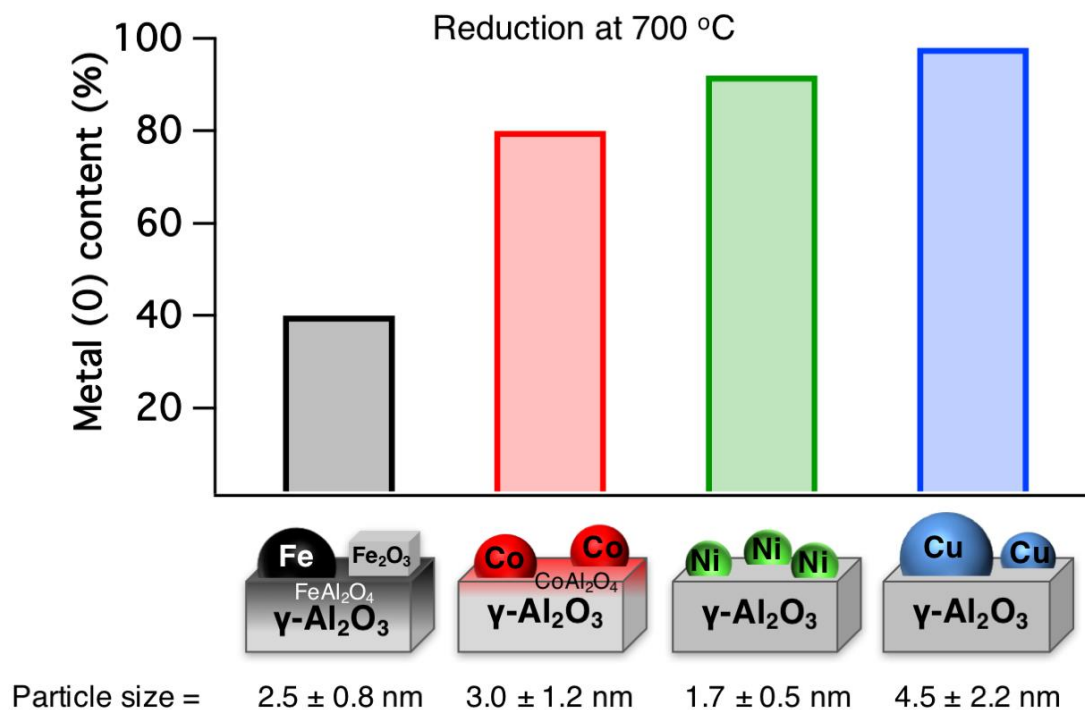


**Figure 7.** Metal (0) content (%) at 700 °C for the different samples determined from LCF of the XANES spectra at the respective metal edge.

## Conclusions

We have developed the synthesis of 3d metal(II) formate precursors that are convenient for the preparation of small supported nanoparticles using  $\gamma$ -alumina as a prototypical support. The synthesis of the metal formate complexes can be easily carried out on gram scale. Upon specific adsorption of these different metal(II) complexes onto dehydroxylated alumina, the metal centers retain their coordination environment (octahedral) and nuclearity, and this approach provides access to high metal loading of approximately 1 precursor.nm<sup>-2</sup> for all systems. After treatment under hydrogen flow at high temperatures, small and narrowly distributed nanoparticles are formed: iron ( $2.5 \pm 0.8$  nm), cobalt ( $3.0 \pm 1.2$  nm), nickel ( $1.7 \pm 0.5$  nm) and Cu ( $2.1 \pm 1.5$  nm), but with their different specificities that follows the reducibility of

the metal: 1) the more easily reducible Cu provides Cu(0) nanoparticles at 500 °C, which increase in size upon increasing the temperature of thermal treatment, 2) then Ni provides small Ni(0) particles in a broader range of temperature along with some residual Ni(II) sites, 3) Co follows with an increasing amount of irreducible Co(II) sites, and 4) finally Fe, the more difficult metal to reduce in the series, requires much higher temperature to generate Fe(0) nanoparticles at the expense of suffering from particle sintering.

## **Experimental Section**

### *General procedure.*

Iron powder (99 %), nickel carbonate (99 %), copper formate (99 %) and formic acid (99 %) were purchased from Sigma-Aldrichs and Alfa Aesar. Co and Cu complexes were prepared without particular precautions, while the synthesis of the Fe complex was performed using Schlenk technique due to the sensitivity of  $\text{Fe}(\text{OCHO})_2 \cdot 2\text{H}_2\text{O}$  towards  $\text{O}_2$ .<sup>[56]</sup> De-ionized water was purified using a Purilab instrument ( $> 10 \text{ M}\Omega\cdot\text{cm}$ ). Deionized water and formic acid solutions were degassed for 2h under flow of argon. Extra dry-acetonitrile™ (99.9 %) was purchased from Acros. Toluene was purified using double MBraun SPS alumina columns and degassed by argon-bubbling for at least 15 min prior to use. The solvents were stored over molecular sieves. Specific adsorptions were carried out using a Schlenk line with Ar (grade 4.5) and  $10^{-3}$  mbar vacuum.

### *Support preparation and characterization*

Alumina nanospheres (NanoSphere) were purchased from Alfa Aesar, NanoDur® with a particle size ranging from 40 nm to 50 nm. The powder XRD pattern shows the presence of a  $\gamma$ -alumina crystalline phase (Figure S2). The BET surface area was estimated at  $32 \text{ m}^2\cdot\text{g}^{-1}$  for NanoSphere material. Prior to use, 6 g of powder was calcined at 500 °C for 12 h ( $5 \text{ }^\circ\text{C}\cdot\text{min}^{-1}$ ) under synthetic air flow ( $100 \text{ mL}\cdot\text{min}^{-1}$ ), degassed under high vacuum ( $10^{-5}$  mbar) at room temperature for 15 min and stored in a glovebox. As

previously reported by Wischert et al., Alumina dehydroxylated at 500 °C has a OH surface concentration of 2 per nm<sup>2</sup>.<sup>[52]</sup>

Physisorption of N<sub>2</sub>. Nitrogen isotherms at -196 °C were measured on a Bel-Mini apparatus from Bel-Japan. Before measurement, the samples were outgassed under vacuum (ca. 10<sup>-3</sup> mbar) at 350 °C for 2 h. The BET method<sup>[57]</sup> was applied to calculate the total surface area.

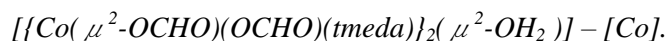
XRD. The X-Ray Diffraction (XRD) measurements were performed using a Bruker-AXS “D8 Advance” diffractometer using Cu K $\alpha$  monochromatic radiation ( $\lambda = 1.5418 \text{ \AA}$ ). The XRD patterns were recorded between 10-80° (2  $\theta$  with a 0.033° step). The samples were analyzed in the form of a finely crushed powder.

#### *Precursor complexes preparation*

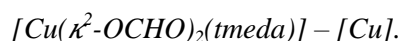
The [ $\{\text{Ni}(\mu^2\text{-OCHO})(\text{OCHO})(\text{tmeda})\}_2(\mu^2\text{-OH}_2)$ ] precursor [**Ni**] was prepared as previously reported.<sup>[7]</sup>



To the iron powder (2 g, 0.036 mol) was added in 85 mL of aqueous formic acid (1.55 M, 0.13 mol). After stirring the reaction mixture under reflux for 2 h, it was filtered to afford a light green solution to which formic acid (5 mL, 0.13 mol) was added. The reaction mixture was taken to dryness under vacuum to afford Fe(OCHO)<sub>2</sub>·2H<sub>2</sub>O (5.25 g, 80%, 37 mmol).<sup>[56]</sup> Tetramethylethylenediamine (1.82 mL, 12 mmol) was added to a clear solution of Fe(OCHO)<sub>2</sub>·2H<sub>2</sub>O (1g, 5.5 mmol) in absolute ethanol (30 mL), leading to a color change to yellow. The reaction mixture was stirred for 5 min, before being taken to dryness. It was extracted with toluene (3 x 10 mL), concentrated to reach saturation of the solution and crystallized at -38°C to afford large light yellow crystals of [ $\{\text{Fe}(\mu^2\text{-OCHO})(\text{OCHO})(\text{tmeda})\}_4$ ] (0.3 g, 1.2 mmol, yield = 22 %) suitable for X-ray crystallography. CCDC 1834512 contains the supplementary crystallographic data. Two successive recrystallizations in toluene lead to the formation of 0.45 g (yield = 33 %, 1.8 mmol). Anal. Calcd (%) for C<sub>28</sub>H<sub>68</sub>Fe<sub>4</sub>N<sub>8</sub>O<sub>16</sub>: C = 33.75 %, H = 6.83 %, N = 11.25 %. Found: C = 33.60 %, H = 6.92 %, N = 10.95 %.



Formic acid (10 mL, 277 mmol) was added to a solution of  $Co(CO_3)$  (5.1g, 43 mmol) in deionized water (100 mL). The reaction mixture was stirred under reflux for 4 h, affording a pink solution. The solution was taken to dryness, treated with absolute ethanol (100 mL) and dried under vacuum ( $10^{-2}$  mbar) to yield  $Co(OCHO)_2 \cdot 2H_2O$  (7 g, 86%, 37 mmol).<sup>[58]</sup> Tetramethylethylenediamine (7.6 mL, 50 mmol) was added to a clear solution of  $Co(OCHO)_2 \cdot 2H_2O$  in deionized water (4.0 g, 22 mmol, 100 mL), leading to a pink solution. The reaction mixture turned dark blue while a flocculent precipitate appeared, before finally turning red-brown. The reaction mixture was taken to dryness and extracted with toluene (150 mL). Concentration of the filtrate and crystallization at  $-38$  °C yielded large pink-purple crystals of [Co] (1.5 g, yield = 24.3 %) suitable for X-ray crystallography. CCDC 1834517 contains the supplementary crystallographic data. Two successive recrystallizations from toluene lead to the formation of 2.1 g (yield = 34%, 7.5 mmol). Coordinating solvents such as tetrahydrofuran and diethylether decoordinates the tetramethylethylenediamine from the metal center. Anal. Calcd (%) for  $C_{16}H_{38}Co_2N_4O_9$ : C = 35.05 %, H = 6.98 %, N = 10.22 %. Found: C = 34.95 %, H = 6.73 %, N = 9.93 %. IR (KBr): 3015, 2981, 2888, 2843, 2818, 2800, 2781, 2733, 2697, 1645, 1563, 1465,  $1366\text{ cm}^{-1}$ .



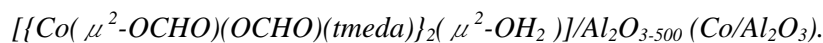
Tetramethylethylenediamine (1.4 mL, 9.2 mmol) was added to a 30-mL blue solution of  $Cu(OCHO)_2 \cdot 4H_2O$  in deionized water (0.98 g, 4.3 mmol), leading to a dark blue solution. The reaction mixture was taken to dryness and extracted with acetonitrile (30 mL). Concentration of the filtrate and crystallization at  $-38$  °C yielded large blue crystals of [Cu] (0.85 g, 3.2 mmol, yield = 75 %) suitable for X-ray crystallography. CCDC 1834516 contains the supplementary crystallographic data. Anal. Calcd (%) for  $C_8H_{18}CuN_2O_4$ : C = 35.62 %, H = 6.72 %, N = 10.38 %. Found: C = 35.34 %, H = 6.56 %, N = 10.11 %. IR (KBr): 3157, 3019, 3004, 2984, 2929, 2855, 2723, 2616, 1590, 1563, 1461,  $1368\text{ cm}^{-1}$ .

*Specific adsorption of [Fe], [Co], [Ni] and [Cu] onto Alumina*

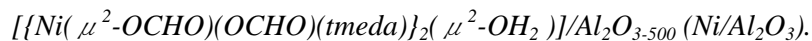




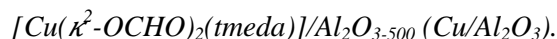
The compound [**Fe**] (120 mg, 0.12 mmol, 0.3 equiv) was dissolved in acetonitrile (40 mL) and contacted with 2.0 g of NanoSphere  $\text{Al}_2\text{O}_{3-500}$  (0.36 mmol  $\text{AlOH}$ , 1 equiv). Upon reaction, a gas release was observed in the solution. The reaction mixture was gently stirred for 2 h at room temperature. The solid was washed 3 times with 20 mL of acetonitrile and dried under vacuum ( $10^{-5}$  mbar) for 16 h to yield a white solid. IR: 3510, 3013, 2976, 2876, 2845, 2805, 2735, 1665, 1368  $\text{cm}^{-1}$ . Elemental analysis: Fe = 0.82 %, C = 0.60 %, H = 0.18 %, N < 0.2 %, which corresponds to the molar ratio of N/Fe > 1 and C/Fe = 3.4.



The compound [**Co**] (172 mg, 0.3 mmol, 0.83 equiv) was dissolved in toluene (20 mL) and contacted with 2.0 g of NanoSphere  $\text{Al}_2\text{O}_{3-500}$  (0.36 mmol  $\text{AlOH}$ , 1 equiv). The reaction mixture was gently stirred for 2 h at room temperature. The solid was washed 3 times with 20 mL toluene and dried under vacuum ( $10^{-5}$  mbar) for 16 h to yield a magenta solid. FTIR ( $\text{cm}^{-1}$ ): 3556, 3016, 2980, 2892, 2848, 2732, 1643, 1610, 1470, 1370. Elemental analysis: Co = 0.80 %, C = 0.72 %, H = 0.18 %, N = 0.26 % with molar ratio of N/Co = 1.4 and C/Co = 4.4.



The compound [**Ni**] (189 mg, 0.35 mmol, 0.97 equiv) was dissolved in toluene (20 mL) and contacted with 2.0 g of NanoSphere  $\text{Al}_2\text{O}_{3-500}$  (0.36 mmol  $\text{AlOH}$ , 1 equiv). The reaction mixture was gently stirred for 2 h at room temperature. The solid was washed 3 times with 20 mL of toluene and dried under vacuum ( $10^{-5}$  mbar) for 16 h to yield a light green solid. FTIR ( $\text{cm}^{-1}$ ): 3669, 3548, 2980, 2881, 2849, 2731, 1662, 1610, 1470, 1394, 1368. Elemental analysis: Ni = 0.58 %, C = 0.70 %, H = 0.19 %, N = 0.26 % with molar ratio of N/Ni = 1.7 and C/Ni = 5.6.



The compound [**Cu**] (100 mg, 0.38 mmol, 1.05 equiv) was dissolved in acetonitrile (20 mL) and contacted with 2.0 g NanoSphere of Al<sub>2</sub>O<sub>3-500</sub> (0.36 mmol AlOH, 1 equiv). The reaction mixture was gently stirred for 2 h at room temperature. The solid was washed 3 times with 20 mL of acetonitrile and dried under vacuum (10<sup>-5</sup> mbar) for 16 h to yield a light green solid. FTIR (cm<sup>-1</sup>): 3543,3018, 2979, 2899, 2854,1687, 1636, 1608 and 1471. Elemental analysis: Cu = 0.36 %, C = 0.43 %, H = 0.18 %, N <0.2 % with molar ratio of N/Cu < 2 and C/Cu = 6.

#### *Reduction of the impregnated materials to give supported nanoparticles*

The dried samples were reduced under a flow of pure hydrogen at 500 °C, 700 °C, 900 °C (1 °C.min<sup>-1</sup>) for 8 h. After outgassing under high vacuum (10<sup>-5</sup> mbar), the catalysts were stored in an Ar atmosphere in a solvent-free glovebox. The code **Metal**<sub>Temperature</sub> refers to the type of metal nanoparticle of the reduced supported nanoparticles and the number in subscript to the reduction temperature.

#### *Scanning Transmission Electron Microscopy (TEM/STEM) study.*

Prior to TEM analysis, all samples were oxidized by the slow diffusion of air to the catalysts under argon. After oxidation, the materials were dispersed in ethanol and a droplet of the suspension was deposited on a lacey carbon foil supported on a copper grid. Scanning transmission electron microscopy images were recorded on an aberration-corrected Hitachi HD2700CS microscope with a high-angle annular dark field detector (HAADF STEM). Particle size distribution (PSD) was determined by analyzing 100 nanoparticles and fitting a normal distribution (particle size = mean value ± standard deviation). X-ray spectra were measured with an energy-dispersive detector (EDX) attached to the HD2700CS. Particle size distributions and EDX spectra are shown in the supplementary information (Figure S9-S15). The metal nanoparticles appear bright in the HAADF-STEM images as Ni has the highest atomic number (Z contrast) among the elements present, which was also confirmed by EDX spectroscopy.

#### *UV-vis.*

UV-visible spectra of the metal salt solutions were recorded with a resolution of 1 nm in the transmission mode on an Agilent Technologies, Cary Series using the corresponding solvent as a reference. UV-visible spectra of the solids were recorded in the reflectance mode (1-nm resolution) on the same spectrometer, using KBr as a reference. The spectra were collected in an air-free cell which was loaded inside the glovebox. The diffuse reflectance spectra were submitted to the Kubelka-Munk transform.

*XAS.*

X-ray absorption spectroscopy (XAS) experiments were performed at the Swiss-Norwegian Beamlines (SNBL, BM31) at the European Synchrotron Radiation Facility (ESRF). XAS spectra were collected at the Fe, Co, Ni and Cu K-edges using a double-crystal Si (111) monochromator (continuous scanning in transmission mode). Calibration of the beamline was performed using metal reference foil and MetalAl<sub>2</sub>O<sub>4</sub> reference. XAS transmission mode spectra were detected using ion chambers filled with He-N<sub>2</sub> gas mixtures. Inside the glovebox, 20mg of powder sample were pressed into 1 cm ring and sealed into a 4cm x 4 cm aluminum bag. EXAFS data were fitted in R-space (1-3.7 Å) after a Fourier transform ( $k = 2 - 10.5 \text{ \AA}^{-1}$ ) using a  $k$  weight of 1, 2 and 3 for the molecular precursors and the grafted species. XANES spectra of the supported nanoparticles were fitted using a linear combination fitting of Metal foil and MetalAl<sub>2</sub>O<sub>4</sub> references for cobalt, nickel and copper-based samples. In the case of iron-based samples, Fe/Al<sub>2</sub>O<sub>3</sub> was fitted with [Fe]-complex, Fe foil and Fe<sub>2</sub>O<sub>3</sub> references. Fe<sub>700</sub> was fitted with Fe foil, FeO and Fe<sub>2</sub>O<sub>3</sub> references.

*TPRd studies.*

These experiments were carried out using a BELCAT-B from BEL JAPAN equipped with a homemade cell allowing the transfer of the sample from the glovebox to the machine without air exposure. 100 mg of dried sample was introduced into the cell. Prior cell opening to the machine, the entry and outlet tubings were purged with Argon for 30 min using a by-pass system. The TPR decomposition measurement was performed from 25 °C to 900 °C, under 6% H<sub>2</sub>/94% He using a ramp of 1 °C.min<sup>-1</sup>. The released gas was followed using a calibrated TCD detector and a mass-spectrometer (Bel-Mass).

### *Single crystal XRD.*

The data were collected on a Bruker D8 Venture diffractometer equipped with a CCD area detector using Mo K $\alpha$  radiation. The crystal was placed in Paratone and mounted in the beam under a flow of nitrogen at 100 K. An empirical absorption correction was performed with SADABS-2008/1 (Bruker). The structure was solved with SHELXL<sup>[59]</sup> using intrinsic phasing followed by a least-squares refinement (SHELXL-97) using the OLEX 2–1.2 suite of programs.<sup>[60]</sup> The non-hydrogen atoms were refined anisotropically. The hydrogen atoms were placed at the calculated positions (see the Supporting Information file for details).

### **Supplementary Material**

Supporting information for this article is available on the WWW under <http://dx.doi.org/10.1002/MS-number>.

### **Acknowledgements**

This research was funded by the Swiss National Funding (SNF) in relation with Swiss Competence Centers for Energy Research (SCCER Heat and Electricity Storage). We are grateful to the European Synchrotron Radiation Facility, Grenoble, France for providing synchrotron radiation beam time at beamline BM31 (31-01-6) of the SNBL and would like to thank Dr. Wouter Van Beek for assistance. We thank Dr. Nikolaos Tsakoumis for providing reference material for XAS measurements. We thank Dr. Frank Krumeich for the STEM measurement and ScopeM (ETH Zürich) for providing measuring time.

### **References**

- [1] F. Zaera, ‘Nanostructured materials for applications in heterogeneous catalysis’, *Chem. Soc. Rev.* **2013**, *42*, 2746-2762.
- [2] P. Barbaro, V. D. Santo, F. Liguori, ‘Emerging strategies in sustainable fine-chemical synthesis: asymmetric catalysis by metal nanoparticles’, *Dalton Trans.* **2010**, *39*, 8391-8402.

- [3] A. Roucoux, J. Schulz, H. Patin, 'Reduced Transition Metal Colloids: A Novel Family of Reusable Catalysts?', *Chem. Rev.* **2002**, *102*, 3757-3778.
- [4] L. C. Buelens, V. V. Galvita, H. Poelman, C. Detavernier, G. B. Marin, 'Super-dry reforming of methane intensifies CO<sub>2</sub> utilization via Le Chatelier's principle', *Science* **2016**, *354*, 449-452.
- [5] B. L. Farrell, V. O. Igenegbai, S. Linic, 'A Viewpoint on Direct Methane Conversion to Ethane and Ethylene Using Oxidative Coupling on Solid Catalysts', *ACS Catal.* **2016**, *6*, 4340-4346.
- [6] S. M. Kim, P. M. Abdala, T. Margossian, D. Hosseini, L. Foppa, A. Armutlulu, W. van Beek, A. Comas-Vives, C. Copéret, C. Müller, 'Cooperativity and Dynamics Increase the Performance of NiFe Dry Reforming Catalysts', *J. Am. Chem. Soc.* **2017**, *139*, 1937-1949.
- [7] T. Margossian, K. Larmier, S. M. Kim, F. Krumeich, A. Fedorov, P. Chen, C. R. Müller, C. Copéret, 'Molecularly Tailored Nickel Precursor and Support Yield a Stable Methane Dry Reforming Catalyst with Superior Metal Utilization', *J. Am. Chem. Soc.* **2017**, *139*, 6919-6927.
- [8] T. Margossian, K. Larmier, S. M. Kim, F. Krumeich, C. Müller, C. Copéret, 'Supported Bimetallic NiFe Nanoparticles through Colloid Synthesis for Improved Dry Reforming Performance', *ACS Catal.* **2017**, *7*, 6942-6948.
- [9] P. Wang, G. Zhao, Y. Wang, Y. Lu, 'MnTiO<sub>3</sub>-driven low-temperature oxidative coupling of methane over TiO<sub>2</sub>-doped Mn<sub>2</sub>O<sub>3</sub>-Na<sub>2</sub>WO<sub>4</sub>/SiO<sub>2</sub> catalyst', *Sci. Adv.* **2017**, *3*.
- [10] Y. Wang, S. De, N. Yan, 'Rational control of nano-scale metal-catalysts for biomass conversion', *Chem. Commun.* **2016**, *52*, 6210-6224.
- [11] P. S. Shuttleworth, M. De bruyne, H. L. Parker, A. J. Hunt, V. L. Budarin, A. S. Matharu, J. H. Clark, 'Applications of nanoparticles in biomass conversion to chemicals and fuels', *Green Chem.* **2014**, *16*, 573-584.

- [12] A. Fedorov, H.-J. Liu, H.-K. Lo, C. Copéret, 'Silica-Supported Cu Nanoparticle Catalysts for Alkyne Semihydrogenation: Effect of Ligands on Rates and Selectivity', *J. Am. Chem. Soc.* **2016**, *138*, 16502-16507.
- [13] M. Guo, H. Li, Y. Ren, X. Ren, Q. Yang, C. Li, 'Improving Catalytic Hydrogenation Performance of Pd Nanoparticles by Electronic Modulation Using Phosphine Ligands', *ACS Catal.* **2018**, *8*, 6476-6485.
- [14] R. C. Reuel, C. H. Bartholomew, 'Effects of support and dispersion on the CO hydrogenation activity/selectivity properties of cobalt', *J. Catal.* **1984**, *85*, 78-88.
- [15] M. Shekhar, J. Wang, W.-S. Lee, W. D. Williams, S. M. Kim, E. A. Stach, J. T. Miller, W. N. Delgass, F. H. Ribeiro, 'Size and Support Effects for the Water-Gas Shift Catalysis over Gold Nanoparticles Supported on Model Al<sub>2</sub>O<sub>3</sub> and TiO<sub>2</sub>', *J. Am. Chem. Soc.* **2012**, *134*, 4700-4708.
- [16] G. L. Bezemer, J. H. Bitter, H. P. C. E. Kuipers, H. Oosterbeek, J. E. Holewijn, X. Xu, F. Kapteijn, A. J. van Dillen, K. P. de Jong, 'Cobalt Particle Size Effects in the Fischer-Tropsch Reaction Studied with Carbon Nanofiber Supported Catalysts', *J. Am. Chem. Soc.* **2006**, *128*, 3956-3964.
- [17] D. Pakhare, J. Spivey, 'A review of dry (CO<sub>2</sub>) reforming of methane over noble metal catalysts', *Chem. Soc. Rev.* **2014**, *43*, 7813-7837.
- [18] L. Foppa, T. Margossian, S. M. Kim, C. Müller, C. Copéret, K. Larmier, A. Comas-Vives, 'Contrasting the Role of Ni/Al<sub>2</sub>O<sub>3</sub> Interfaces in Water-Gas Shift and Dry Reforming of Methane', *J. Am. Chem. Soc.* **2017**, *139*, 17128-17139.
- [19] H. Tang, F. Liu, J. Wei, B. Qiao, K. Zhao, Y. Su, C. Jin, L. Li, J. Liu, J. Wang, T. Zhang, 'Ultrastable Hydroxyapatite/Titanium-Dioxide-Supported Gold Nanocatalyst with Strong Metal-Support Interaction for Carbon Monoxide Oxidation', *Angew. Chem. Int. Ed.* **2016**, *55*, 10606-10611.

- [20] D. Gajan, K. Guillois, P. Delichère, J.-M. Basset, J.-P. Candy, V. Caps, C. Coperet, A. Lesage, L. Emsley, 'Gold Nanoparticles Supported on Passivated Silica: Access to an Efficient Aerobic Epoxidation Catalyst and the Intrinsic Oxidation Activity of Gold', *J. Am. Chem. Soc.* **2009**, *131*, 14667-14669.
- [21] K. Furman, D. Baudouin, T. Margossian, K. D. Sabnis, Y. Cui, F. H. Ribeiro, C. Copéret, 'Increased methanation activity through passivation of the silica support', *J. Catal.* **2015**, *324*, 9-13.
- [22] D. Baudouin, U. Rodemerck, F. Krumeich, A. de Mallmann, K. C. Szeto, H. Ménard, L. Veyre, J.-P. Candy, P. B. Webb, C. Thieuleux, 'Particle size effect in the low temperature reforming of methane by carbon dioxide on silica-supported Ni nanoparticles', *J. Catal.* **2013**, *297*, 27-34.
- [23] A. Khodakov, W. Chu, P. Fongarland, 'Recent advances in the liquid-phase syntheses of inorganic nanoparticles, advances in the development of novel cobalt Fischer–Tropsch catalysts for synthesis of long-chain hydrocarbons and clean fuels', *Chem. Rev.* **2007**, *107*, e744.
- [24] K. Murata, Y. Mahara, J. Ohyama, Y. Yamamoto, S. Arai, A. Satsuma, 'The Metal–Support Interaction Concerning the Particle Size Effect of Pd/Al<sub>2</sub>O<sub>3</sub> on Methane Combustion', *Angew. Chem. Int. Ed.* **2017**, *56*, 15993-15997.
- [25] X. Carrier, J.-B. d'Espinose de la Caillerie, J.-F. Lambert, M. Che, 'The Support as a Chemical Reagent in the Preparation of WO<sub>x</sub>/γ-Al<sub>2</sub>O<sub>3</sub> Catalysts: Formation and Deposition of Aluminotungstic Heteropolyanions', *J. Am. Chem. Soc.* **1999**, *121*, 3377-3381.
- [26] J.-B. d'Espinose de la Caillerie, M. Kermarec, O. Clause, 'Impregnation of γ-Alumina with Ni (II) or Co (II) Ions at Neutral pH: Hydrotalcite-Type Coprecipitate Formation and Characterization', *J. Am. Chem. Soc.* **1995**, *117*, 11471-11481.
- [27] J. Abi Aad, P. Courty, D. Decottignies, M. Michau, F. Diehl, X. Carrier, E. Marceau, 'Inhibition by Inorganic Dopants of γ-Alumina Chemical Weathering under Hydrothermal Conditions:

Identification of Reactive Sites and their Influence in Fischer–Tropsch Synthesis’, *ChemCatChem* **2017**, *9*, 2106-2117.

[28] Y. Chen, D.-L. Peng, D. Lin, X. Luo, ‘Preparation and magnetic properties of nickel nanoparticles via the thermal decomposition of nickel organometallic precursor in alkylamines’, *Nanotechnology* **2007**, *18*, 505703.

[29] A. Gojova, B. Guo, R. S. Kota, J. C. Rutledge, I. M. Kennedy, A. I. Barakat, ‘Induction of inflammation in vascular endothelial cells by metal oxide nanoparticles: effect of particle composition’, *Environ. Health Perspect.* **2007**, *115*, 403.

[30] F. Meshkani, M. Rezaei, ‘Simplified direct pyrolysis method for preparation of nanocrystalline iron based catalysts for H<sub>2</sub> purification via high temperature water gas shift reaction’, *Chem. Eng. Res. Des.* **2015**, *95*, 288-297.

[31] B. AlSabban, L. Falivene, S. M. Kozlov, A. Aguilar-Tapia, S. Ould-Chikh, J.-L. Hazemann, L. Cavallo, J.-M. Basset, K. Takanabe, ‘In-operando elucidation of bimetallic CoNi nanoparticles during high-temperature CH<sub>4</sub>/CO<sub>2</sub> reaction’, *Appl. Catal., B* **2017**, *213*, 177-189.

[32] J. Schumann, T. Lunkenbein, A. Tarasov, N. Thomas, R. Schlögl, M. Behrens, ‘Synthesis and characterisation of a highly active Cu/ZnO: Al catalyst’, *ChemCatChem* **2014**, *6*, 2889-2897.

[33] A. Y. Khodakov, W. Chu, P. Fongarland, ‘Advances in the development of novel cobalt Fischer–Tropsch catalysts for synthesis of long-chain hydrocarbons and clean fuels’, *Chem. Rev.* **2007**, *107*, 1692-1744.

[34] V. Rodriguez-Gonzalez, E. Marceau, P. Beaunier, M. Che, C. Train, ‘Stabilization of hexagonal close-packed metallic nickel for alumina-supported systems prepared from Ni (II) glycinate’, *J. Solid State Chem.* **2007**, *180*, 22-30.



- [35] F. Bentaleb, M. Che, A.-C. Dubreuil, C. Thomazeau, E. Marceau, 'Influence of organic additives on the properties of impregnation solutions and on nickel oxide particle size for Ni/Al<sub>2</sub>O<sub>3</sub> catalysts', *Catal. Today* **2014**, 235, 250-255.
- [36] F. Negrier, É. Marceau, M. Che, D. de Caro, 'Role of ethylenediamine in the preparation of alumina-supported Ni catalysts from [Ni(en)<sub>2</sub>(H<sub>2</sub>O)<sub>2</sub>](NO<sub>3</sub>)<sub>2</sub>: from solution properties to nickel particles', *C. R. Chim.* **2003**, 6, 231-240.
- [37] F. Dumond, E. Marceau, M. Che, 'A Study of Cobalt Speciation in Co/Al<sub>2</sub>O<sub>3</sub> Catalysts Prepared from Solutions of Cobalt–Ethylenediamine Complexes', *The Journal of Physical Chemistry C* **2007**, 111, 4780-4789.
- [38] A. Davantès, C. Schlaup, X. Carrier, M. Rivallan, G. Lefèvre, 'In Situ Cobalt Speciation on  $\gamma$ -Al<sub>2</sub>O<sub>3</sub> in the Presence of Carboxylate Ligands in Supported Catalyst Preparation', *Journal of Physical Chemistry C* **2017**, 121, 21461-21471.
- [39] K. Mori, K. Miyawaki, H. Yamashita, 'Ru and Ru–Ni Nanoparticles on TiO<sub>2</sub> Support as Extremely Active Catalysts for Hydrogen Production from Ammonia–Borane', *ACS Catal.* **2016**, 6, 3128-3135.
- [40] N. E. Tsakoumis, J. C. Walmsley, M. Rønning, W. van Beek, E. Rytter, A. Holmen, 'Evaluation of Reoxidation Thresholds for  $\gamma$ -Al<sub>2</sub>O<sub>3</sub>-Supported Cobalt Catalysts under Fischer–Tropsch Synthesis Conditions', *J. Am. Chem. Soc.* **2017**, 139, 3706-3715.
- [41] J. P. Dacquin, D. Sellam, C. Batiot - Dupeyrat, A. Tougerti, D. Duprez, S. Royer, 'Efficient and robust reforming catalyst in severe reaction conditions by nanoprecursor reduction in confined space', *ChemSusChem* **2014**, 7, 631-637.
- [42] K. Larmier, W. C. Liao, S. Tada, E. Lam, R. Verel, A. Bansode, A. Urakawa, A. Comas - Vives, C. Copéret, 'CO<sub>2</sub> - to - Methanol Hydrogenation on Zirconia - Supported Copper Nanoparticles:

Reaction Intermediates and the Role of the Metal-Support Interface', *Angew. Chem. Int. Ed.* **2017**, *56*, 2318-2323.

[43] S. Tada, K. Larmier, R. Büchel, C. Copéret, 'Methanol synthesis via CO<sub>2</sub> hydrogenation over CuO-ZrO<sub>2</sub> prepared by two-nozzle flame spray pyrolysis', *Catal. Sci. Technol.* **2018**, *8*, 2056-2060.

[44] L. Foppa, M.-C. Silaghi, K. Larmier, A. Comas-Vives, 'Intrinsic reactivity of Ni, Pd and Pt surfaces in dry reforming and competitive reactions: Insights from first principles calculations and microkinetic modeling simulations', *J. Catal.* **2016**, *343*, 196-207.

[45] Z. Li, N. M. Schweitzer, A. B. League, V. Bernales, A. W. Peters, A. B. Getsoian, T. C. Wang, J. T. Miller, A. Vjunov, J. L. Fulton, 'Sintering-resistant single-site nickel catalyst supported by metal-organic framework', *J. Am. Chem. Soc.* **2016**, *138*, 1977-1982.

[46] K. Wefers, 'Alumina chemicals: science and technology handbook', *The American Ceramic Society, Westerville, Ohio* **1990**, *13*.

[47] R. K. Oberlander, Google Patents, 1980.

[48] M. Trueba, S. P. Trasatti, 'γ-Alumina as a support for catalysts: a review of fundamental aspects', *Eur. J. Inorg. Chem.* **2005**, *2005*, 3393-3403.

[49] A. M. Bryan, W. A. Merrill, W. M. Reiff, J. C. Fettinger, P. P. Power, 'Synthesis, Structural, and Magnetic Characterization of Linear and Bent Geometry Cobalt (II) and Nickel (II) Amido Complexes: Evidence of Very Large Spin-Orbit Coupling Effects in Rigorously Linear Coordinated Co<sup>2+</sup>', *Inorg. Chem.* **2012**, *51*, 3366-3373.

[50] A. M. Schmiedekamp, M. D. Ryan, R. J. Deeth, 'Six-coordinate Co<sup>2+</sup> with H<sub>2</sub>O and NH<sub>3</sub> ligands: Which spin state is more stable?', *Inorg. Chem.* **2002**, *41*, 5733-5743.

- [51] R. D. Shannon, 'Revised effective ionic radii and systematic studies of interatomic distances in halides and chalcogenides', *Acta crystallographica section A: crystal physics, diffraction, theoretical and general crystallography* **1976**, *32*, 751-767.
- [52] R. Wischert, P. Laurent, C. Copéret, F. o. Delbecq, P. Sautet, 'γ-Alumina: the essential and unexpected role of water for the structure, stability, and reactivity of "defect" sites', *J. Am. Chem. Soc.* **2012**, *134*, 14430-14449.
- [53] D. P. Estes, G. Siddiqi, F. Allouche, K. V. Kovtunov, O. V. Safonova, A. L. Trigub, I. V. Koptuyg, C. Copéret, 'C-H Activation on Co<sub>3</sub>O<sub>4</sub> Sites: Isolated Surface Sites versus Molecular Analogs', *J. Am. Chem. Soc.* **2016**, *138*, 14987-14997.
- [54] A. Lever, 'Electronic spectra of dn ions', *Inorganic Electronic Spectroscopy* **1984**, *2*, 376-611.
- [55] L. Bonneviot, O. Legendre, M. Kermarec, D. Olivier, M. Che, 'Characterization by UV-vis-NIR reflectance spectroscopy of the exchange sites of nickel on silica', *J. Colloid Interface Sci.* **1990**, *134*, 534-547.
- [56] R. N. Chemical Society Reviews Rhoda, A. V. Fraioli, W. L. Taylor, J. Kleinberg, 'Iron(II) Formate', *Inorg. Synth.* **1953**.
- [57] S. Brunauer, P. H. Emmett, E. Teller, 'Adsorption of gases in multimolecular layers', *J. Am. Chem. Soc.* **1938**, *60*, 309-319.
- [58] A. Kaufman, C. Afshar, M. Rossi, D. E. Zacharias, J. P. Glusker, 'Metal ion coordination in cobalt formate dihydrate', *Struct. Chem.* **1993**, *4*, 191-198.
- [59] G. Sheldrick, 'SHELXT - Integrated space-group and crystal-structure determination', *Acta Crystallogr. Sect. A* **2015**, *71*, 3-8.
- [60] O. V. Dolomanov, L. J. Bourhis, R. J. Gildea, J. A. K. Howard, H. Puschmann, 'OLEX2: a complete structure solution, refinement and analysis program', *J. Appl. Crystallogr.* **2009**, *42*, 339-341.

